Chapter 1

---

1. Introduction

In this chapter, we will deal with very general things, that will serve later as a basis to speak the same "language". The Chapter has three main goals:

- to understand why "classical" scans used by diffractionists, like θ-2θ or ω scans, are not able to provide quantitative information about texture, and many times even not qualitative information.
- to be able to interpret and draw pole figures of typical textures.
- to recognise why we need to calculate another object, called ODF, and not only pole figures, in general.

Used variables:

dS	Surface element of the Pole Sphere
a, b, c, α_c, β_c, γ_c	Unit-cell parameters
a, **b**, **c**	Unit vectors of the unit-cell
Δk	Scattering vector
n	Normal to the sample surface
$\mathcal{S}$	Spectrometer (Diffractometer) space
χ	Polar angle in the diffractometer space
φ	Azimuthal angle in the diffractometer space
$\mathcal{Y}$	Pole figure space
ϑ_y	Polar angle in the pole figure space
φ_y	Azimuth of pole figures
hkℓ	Miller indices
(hkℓ)	Crystallographic plane hkℓ
{hkℓ}	Crystallographic planes hkℓ and diffracting equivalents
[hkℓ]	Crystallographic direction hkℓ
[hkℓ]*	Crystallographic direction hkℓ of the reciprocal space
<hkℓ>	Crystallographic direction hkℓ and diffracting equivalents
<hkℓ>*	Crystallographic direction hkℓ and diffracting equivalents of the reciprocal space
$L_{hk\ell}$	Lotgering factor
p, p_0	ratio entering the Lotgering factor for a textured and a random sample respectively
h	<hkℓ>* directions
y	ϑ_y, φ_y direction in $\mathcal{Y}$
$I_{\mathbf{h}}(\mathbf{y})$	Direct pole figure
$P_{\mathbf{h}}(\mathbf{y})$	Normalised pole figure
K_A	Sample reference frame
($\mathbf{x_A}$, $\mathbf{y_A}$, $\mathbf{z_A}$)	Unit-vectors of the sample reference frame
X_A, Y_A, Z_A	Sample axes aligned with $\mathbf{x_A}$, $\mathbf{y_A}$, $\mathbf{z_A}$ respectively
[XYZ]	Vector of the sample reference frame
($\mathbf{x_B}$, $\mathbf{y_B}$, $\mathbf{z_B}$)	Unit-vectors of the crystal reference frame
X_B, Y_B, Z_B	Sample axes aligned with $\mathbf{x_B}$, $\mathbf{y_B}$, $\mathbf{z_B}$ respectively
$\mathcal{G}$	Orientation space
g	Set of three Euler angles defining one orientation

dg	Orientation element in the $\mathcal{G}$-space
α, β, γ	Euler angles in the $\mathcal{G}$-space in the Roe-Matthies convention
$\varphi_1, \Phi, \varphi_2$	Euler angles in the $\mathcal{G}$-space in the Bunge convention
f(g)	Orientation Distribution Function
$d_{hk\ell}$,	Inter-reticular distance between (hkℓ) planes
ω	Angle between the incident beam and the sample surface: incidence angle
θ	Angle between the incident beam and the scattering planes {hkℓ}: Bragg angle
δ	Angle between the scattering planes and the sample surface
V	Irradiated volume of the sample
dV(**y**)	Volume of crystallites having **h** between **y** and **y** + **dy**
dV(g)	Volume of crystallites which orientation is between g and g + dg

Abbreviations:

CPS	Curved Position Sensitive detector
ESR	Electron Spin Resonance
FWHM	Full Width at Half Maximum
m.r.d.	multiple of a random distribution
NMR	Nuclear Magnetic Resonance
ODF	Orientation Distribution Function
PSD	Position Sensitive Detector
QTA	Quantitative Texture Analysis
SEM	Scanning Electron Microscope
TEM	Transmission Electron Microscope

Notes

Vectors are noted by bold letters
Unless specified, diffraction means "normal diffraction" (opp. anomalous diffraction)
The sign ^ means the vector product

2. Qualitative aspects of crystallographic textures

Natural or artificial solids (rocks, ceramics, metals, alloys ...) are constituted by aggregates of grains of different phases, sizes, shapes and orientations. Grains can be viewed at different scales, depending on the tool used to examine them.

Using metallurgical or geological optical microscopes, grains at the micrometer scale are visible, delimiting areas of different reflection or transmission of light. Since visible light is in a micrometer wavelength range, optics tell us the optical resolution is in the same order of range, and no detail about crystallographic lattices is made accessible, except there are known relationship between grain reflectivity or shape and crystal lattices. This has been used for long by geologists and metallurgists to study crystallographic textures, prior to have access to more sophisticated techniques.

With the development of scanning electron microscopes (SEM), scale ranges down to several nanometers have been made accessible. Since electrons interact mainly with electrons

(at least at low energies), grain contrast are made visible in patterns through differences in atomic numbers. The way the electrons are interacting with the material, and the way the information is detected (as backscattered electrons, x- or γ- emitted rays, inelastic or elastic scattering ...) will condition the relevance of the information to be interpreted for texture analysis. We can reasonably dissociate into two groups of information, if texture only is of concerns, depending if the information is provided through a diffraction process or not.

If no diffraction occurs, the lattice plane spacing in the grains are not probed and the relevant information gives "images" of the grains at the end. If these images are, or not, interpretable as crystallographic texture lies on the same assumptions as for visible microscopy: it has to exist a clear relationship between texture and the probed information.

Dealing with diffraction processes on the contrary probes directly interplanar distances, and allows the texture characterisation. Diffraction of electrons in microscopes (SEM or TEM) for texture studies are generally carried out by examining Kikuchi patterns, but are beyond the scope of this course. Peoples interested in are pleased to read for instance Wright 1993, Wright & Adams 1992, Wenk 1998.

Major advances in Quantitative Texture Analysis (QTA) have been brought by modern diffractometry using x-rays or neutrons. In both cases the wavelength of the radiation is comparable to the lattice sizes, and diffraction patterns can be used to more or less directly determine the texture. We should mention here an important point which makes people running into confusions if they do not pay attention: x-ray or neutron diffraction probe crystallites and not grains. A crystallite is the largest domain which satisfies the periodic translation of the crystal unit-cell in the three dimensional space. Hence, grains as seen by microscopy can be made of a lot of crystallites, and a single-crystal is made of one crystallite. We observed that many people were using grain and crystallite for either both of them, while we are used to neatly dissociate the two terms, as in this text.

Usually, samples of interest are multi-phasic substances, i.e. they contain several crystalline phases of different structure, each phase having its own properties including texture, and with possible interactions between phases. Dealing with anisotropy of the macroscopic properties of the ensemble, the most important parameter, at a few exceptions, will be the texture. Anisotropic crystal structures will produce anisotropy of the polycrystalline material only via the stabilisation of texture of at least one phase. As an exception, we should cite elastic properties, for which even in randomly oriented (isotropic) samples exhibit anisotropy (the one that gives rise to longitudinal and transverse wave velocities for instance). The anisotropy can also come from extrinsic contributions, like for magnetic properties for instance, for which long range interactions and shape effects may create anisotropic magnetic signals of a polycrystal without texture.

But usually, and depending on the technique used to measure a sample property, crystallographic textures may have an important impact. In order to evaluate if this is the case for a specific study before any diffraction experiment, one has to primarily test these options:

- Does the material I am looking at contains at least one crystalline phase ?

Amorphous materials have no long range periodicity of atoms, it is then a nonsense to speak about orientation of crystal axes. Anisotropic properties may be found in amorphous materials, but it is not a crystallographic texture effect. However, some materials are mixtures of crystalline and amorphous phases, the former being potentially textured.

- Are the crystalline systems constituting my materials anisotropic for the physical or chemical property of concerns ?

For instance, cubic crystal systems are isotropic for optical properties, but not for elastic properties.

• Are the crystallites randomly distributed in the sample ?

Even with anisotropic physical properties of the individual crystallites, if these later are randomly distributed, their intrinsic properties too. Take care with elastic properties, which in this case still stay anisotropic.

• Are they some particular effects linked to the properties which I am measuring that make the anisotropy not visible ?

Even if the material is textured and is constituted of anisotropic crystallites, the anisotropy of the measured property may be masked. For instance, the shape of the crystallites may give rise to demagnetising factors that can mask the magnetic macroscopic anisotropy. In spectroscopic techniques (ESR, NMR …), measuring spectra at the so-called "magic angle" can remove completely any effect of the texture …

3. Effects on diffraction diagrams

3.1. θ-2θ diagrams

Figure 1 is a scheme of a classical diffraction arrangement used for powder diffraction. It is generally known as the Bragg-Brentano configuration (Brentano 1946, Cullity 1978). The incident and diffracted beams define the incident plane (scattering plane), in which diffraction is measured, with a scattering vector $\mathbf{\Delta k}$. The detector is placed at an angle 2θ from the incident beam, itself at θ from the sample plane. Using this scan strategy, crystallographic planes of different d-spacings are successively brought into diffraction.

Figure 2a shows a diffraction diagram for a random powder of $La_{0.88}Li_{0.12}TiO_3$, and Figure 2b a diagram for the same phase deposited by sputtering on a (100) oriented MgO single crystal substrate. Since the substrate d-spacings match the film ones, it induces texture of the film, and the peak reflections are no more in the powder ratio. As we will see in next paragraphs, the effect of the texture can only be measured qualitatively with such a single diagram.

However, if the θ-2θ scan strategy reveals peaks from a large range of $d_{hk\ell}$, it only probes those {hkℓ} planes that are parallel to the sample plane.

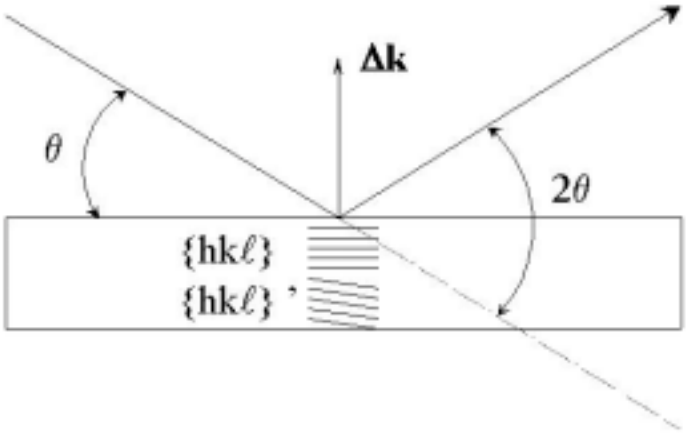

Figure 1: Schematic of a diffraction experiment using the θ-2θ geometry. The plane of the figure is the scattering plane.

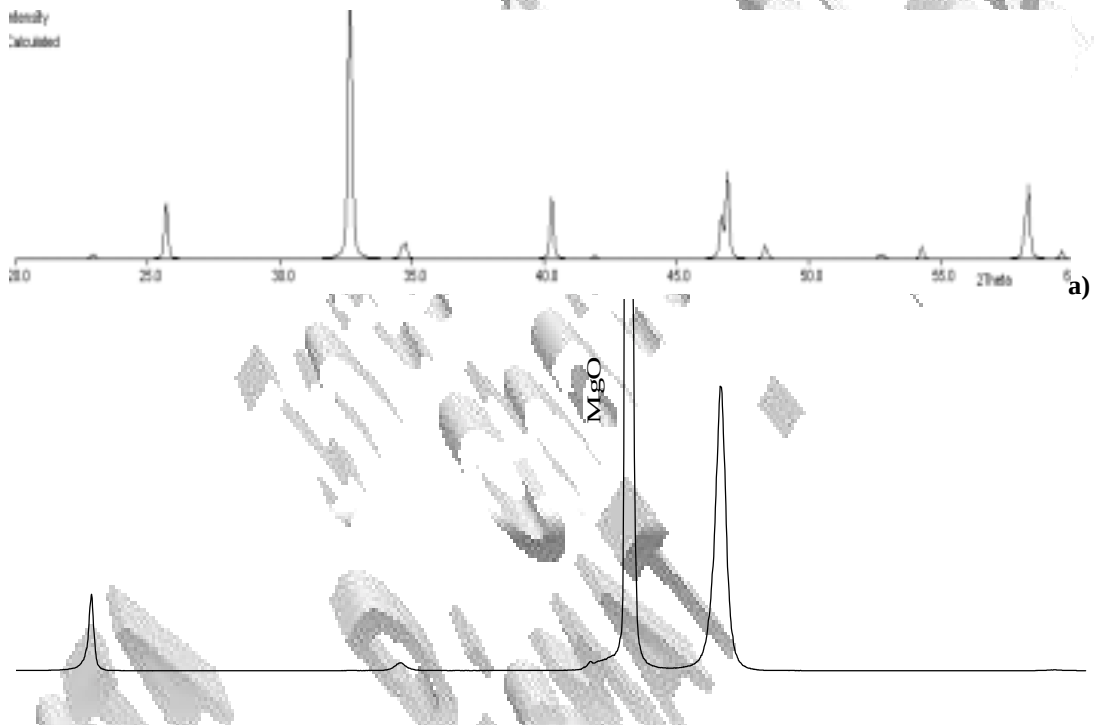

Figure 2: a): Theoretical diagram for bulk $La_{0.88}Li_{0.12}TiO_3$ and **b)**: experimental diagram for the same phase deposited on a (100) oriented MgO single crystal.

3.2. Asymmetric diagrams

Such diagrams are either measured with the same scanning strategy as before, θ-2θ with a point detector, but with the sample rotated to a fixed angle δ relative to its previous position (Figure 3), or using only a 2θ scan, with point or Position Sensitive, linear (PSD) (Wcislak et al. 1993) or curved (CPS) detectors (Heizmann et Laruelle 1986).

In the former case, the diagrams are similar to the ones of Figure 2, if we forget corrections for absorption and volume changes. This diffraction geometry then only probes for {hkℓ}' planes that are inclined by $\delta = \omega - \theta$ from the sample plane, and texture is only measured qualitatively using such a diagram as previously. It can however be used for a qualitative check of the texture, for instance to prepare a texture experiment on another goniometer.

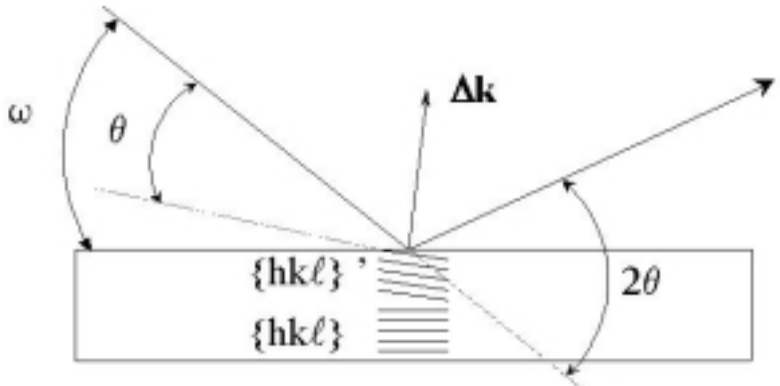

Figure 3: Asymmetric geometry of measurement

In the latter case, only one incident angle ω is used and all the diffracted lines are recorded simultaneously for all the 2θ positions made available by the detector (Figure 4). Then planes that are diffracting at 2θ are not in the same orientation than the ones diffracting at 2θ', ...

The textural information is then a bit more consequent, but only these planes are diffracting. Measuring a flat powder sample, such a set-up will provide a diagram exhibiting all the diffracted lines, with specific defocusing effects that will depend on ω and the detector used. Absorption and volume corrections will also have to be carried out. Diagrams measured on a textured sample will exhibit peak ratio which will depend on the texture, and different than for a Bragg-Brentano measurement.

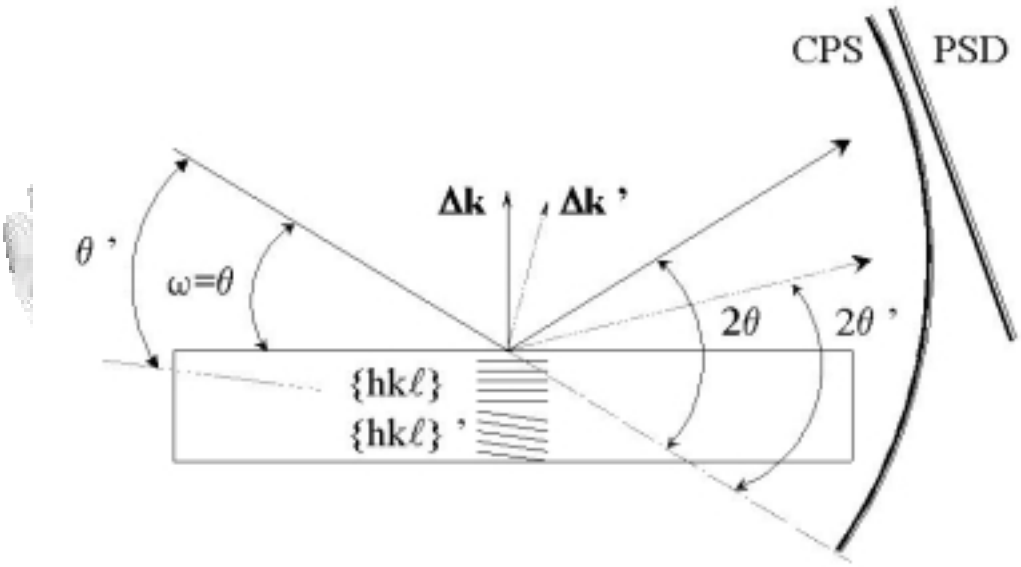

Figure 4: Asymmetric geometry using a PSD or a CPS

For instance, a sample that exhibits only {00ℓ} lines in the Bragg-Brentano geometry may show at maximum only one {00ℓ} peak using the asymmetric set-up (if {002} is diffracting, for the $2\theta_{003}$ peak position the {003} planes are not fulfilling the Bragg law). Of course this is true only if the orientation dispersion is not too large.

Such a set-up is very useful for decreasing the acquisition times, because it economises the scan in θ-2θ. In particular, it is very useful for texture analysis which requires a lot of measured sample orientations. It is then particularly suited for materials having low diffraction yields, like thin films for instance.

3.3. ω-scans: rocking curves

This scan strategy is often used to reveal the orientation of planes with an orientation close to parallel to the sample surface. For a fixed θ-2θ position (Figure 5), planes positioned at different ω-θ are brought to diffraction by varying ω (taken positive for a counter clockwise rotation).

This kind of measurement is most used by single crystal growers in order to check the quality of their single crystals, called mosaic. In this case, the measured planes are inclined by few tenth of a degree at maximum, and no absorption change between several ω positions is significant, at a first approximation. This method is also used more and more to measure the texture of thin structures, although the "mosaic" is then much larger, and often not suited for such a characterisation.

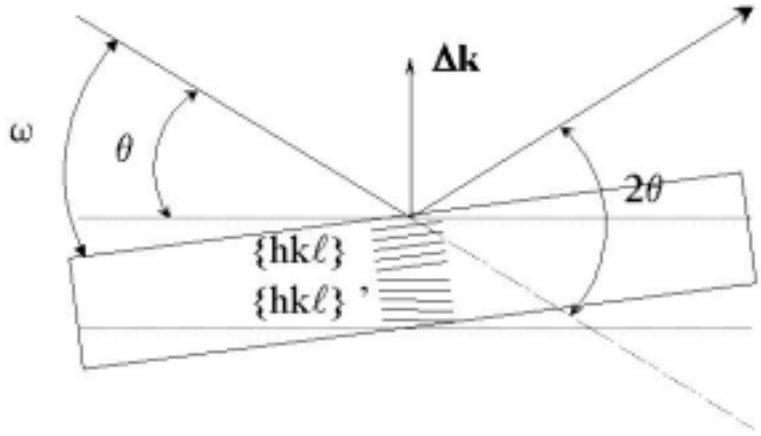

Figure 5: ω-scan (rocking curves arrangement) for measuring orientations

A typical rocking curve of a {002} line measured for a single crystal is presented in Figure 6. The FWHM of this reflection is 0.1° in ω, which means that a certain amount of crystallites are inclined by 0.1° or less. The corresponding volume amount depends on the curve shape. In this example the distribution is represented by a Gaussian, and approximately 86 % of the intensity is within the FWHM.

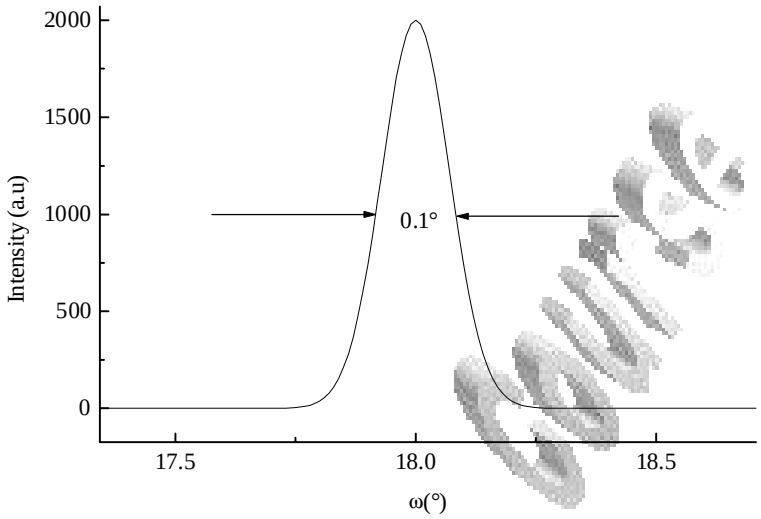

Figure 6: ω-scan of a single crystal having a 0.1° FWHM of its {002} reflection centred at 2θ = 18°

4. Limitations of classical diagrams

4.1. θ-2θ diagrams

It is essential to notice that these diagrams are only probing planes parallel to the sample surface, because this may represent only a low percentage of the volume of the material.

In this kind of experiment, diffraction lines are given by the Bragg's law. The experiment itself may restrict the available range of observed peaks, by construction. Generally, ranges of at best 2θ = 165° are measured. In this range, for a randomly oriented sample, the diamond structure (Fd3m space group, a = 3.566 Å) using Cr $K\alpha_1$ radiation (2.2897 Å) will show only two peaks (Figure 7), corresponding to the {111} and {220} planes. Lets imagine now an oriented sample of diamond in the same conditions. If the orientation is such that all the {100} planes are parallel to the surface of the sample, no diffraction peak will be observed. This is of course an extreme case, with a small, strongly symmetric unit-cell, under a relatively large radiation. But lets now imagine {hkℓ}' planes which could correspond to a texture component with {111} planes tilted with respect to the sample normal. This component will neither have {220} planes parallel to the surface, nor a second texture component with {220} planes tilted from the normal will show {111} diffraction lines. We can then imagine a sample with two texture components not showing any diffraction peak in the available range, and we can extend this reasoning to larger 2θ ranges, larger and less symmetric unit-cells.

The only important question is "how is the texture" ? Depending on the answer, we will have rights to use classical Bragg-Brentano scans to say something about the texture.

Looking at Figure 1 and Figure 8, one can also see that for a given {hkℓ} plane family, any rotation around the sample normal, **n**, does not change the diffraction diagram. If {hkℓ} are parallel to the surface, the diffracted intensity is kept constant, while for {hkℓ}' planes no

intensity is detected. In particular, the two configurations represented in Figure 8 for two different orientations of {hkℓ} planes give the same diffraction diagram. Both texture components have the **c** axes of the structure parallel with **n**, but component C_1 has its **a** axes parallel with the macroscopic edges of the sample, while C_2 has **a** axes at random around **n**. We can conclude from this that it is impossible to check for eventual in-plane alignment of the axes (like developed in epitaxial relationship) for the given sample, only looking at classical θ-2θ diagrams.

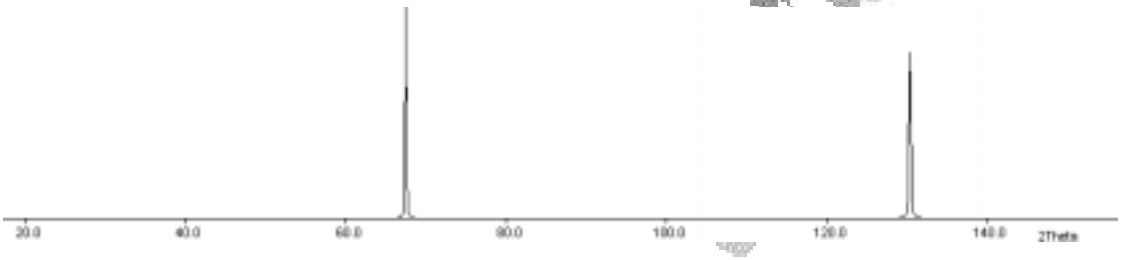

Figure 7: Theoretical diagram in the 20-165° 2θ-range, for diamond measured with Cr $K\alpha_1$ radiation

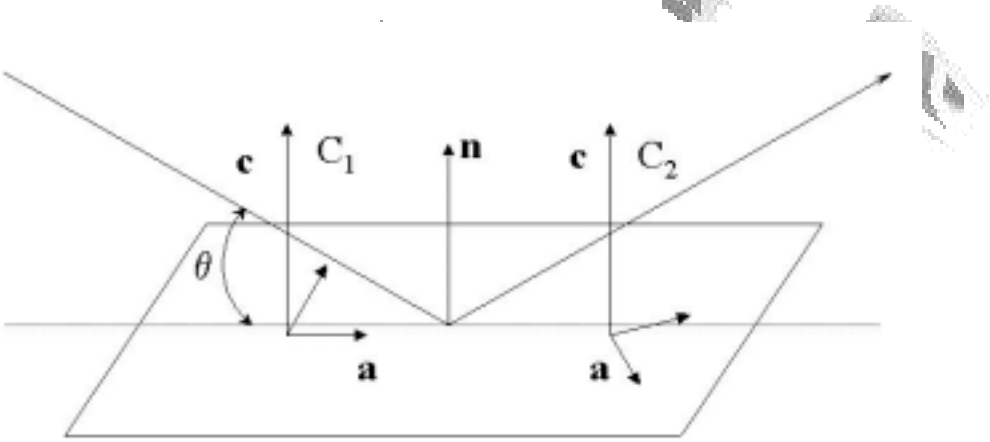

Figure 8: Two texture components differing only by their orientation in the sample plane

It should be mentioned here that semi-quantitative approaches of θ-2θ diagrams in view of quantifying the textures have been developed in the past. The relative ratio of different peaks from a textured diagram can provide information on texture. For instance, Lotgering 1959 derived a quantitative factor, $L_{hk\ell}$, to reveal how strong the texture is in a given material. This factor is defined by:

$$L_{hk\ell} = \frac{p - p_0}{1 - p_0} \qquad (1)$$

where the p factors are calculated, in θ-2θ diagrams only, by the ratio of the sum of specific $I\{hk\ell\}_i$ lines (all $I\{00\ell\}$'s for instance) to the sum of all the lines available in a Δθ range:

$$p = \frac{\sum_i I\{hk\ell\}_i}{\sum_{hk\ell} I\{hk\ell\}} \qquad (2)$$

with p being calculated for the textured sample while p_0 is for a sample without preferred orientation. Then p varies from p_0 for a powder to 1 in an ideally oriented sample, and $L_{hk\ell}$ varies from 0 for a perfect powder to 1 for a fully oriented sample.

However, if this factor is somehow linked to the strength of the texture (and Lotgering specifically advised for it too), it is specific of one kind of planes only. If two or more textures are present at the same time, two factors have to be calculated, with *a priori* no clear relationship between them. Also, this factor is affected by the available $\Delta\theta$ range. Furthermore, it would still neither find any difference between the C_1 and C_2 variants of Figure 8, nor be modified by the dispersion of the component, even if only one component of texture is existing, although the consequences of different dispersions on the physical properties may be drastically different !

4.2. Asymmetric diagrams

The limits developed for the regular θ-2θ scans remain valid for the asymmetric geometry, whatever the detector used. But, a rotation around **n** will be able to provide some information about eventual in-plane alignment since this rotation will bring to diffract planes which are not coplanar (except if $\omega = \theta$, which corresponds to the regular θ-2θ scan).

4.3. ω-scans

This measurement methodology can bring to diffraction, in the limit of reasonable ω's, only planes perpendicular to the incident plane. For instance (Figure 9), planes parallel to the scattering plane will never satisfy the Bragg law when rotating through ω.

The ω-scan strategy may be aimed to quantitatively measure the texture, provided another axis of rotation is added. The combined use of ω and rotation around **n** has been first used by Field et Merchant, 1949, in order to accomplish texture measurements. This method suffers a lack of extent of the available measurements.

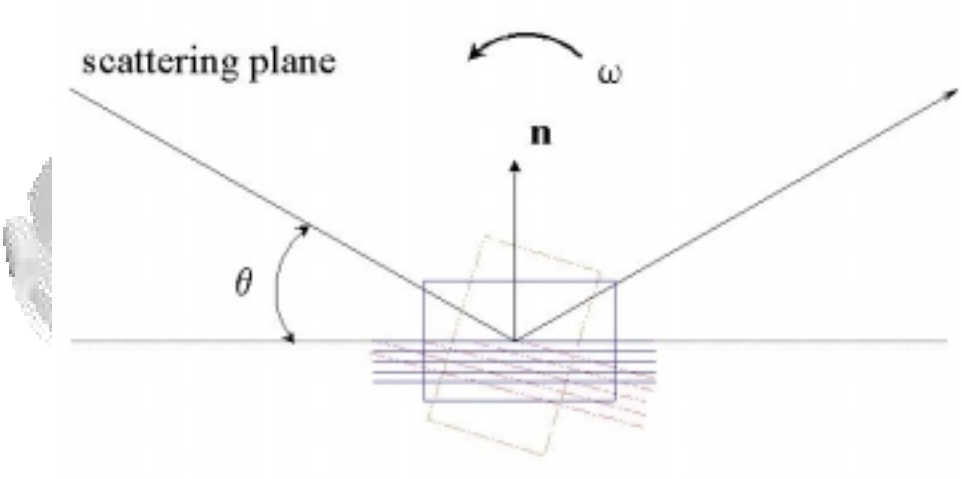

Figure 9: Illustration of crystallographic planes rotation when planes are perpendicular (dotted or continuous lines) or parallel (rectangles) to the diffraction plane

Lets imagine a distribution of crystallites well represented by a Gaussian shape with a FWHM of 30°. In order to bring a plane which makes an angle of $\omega = -30°$ with the sample surface into diffraction conditions, one has to rotate the sample by 30°, means $\omega = \theta + 30$. In

the mean time, if the peak of interest is diffracting at a θ position lower than 30°, the diffracted beam is then fully absorbed in the sample ! In this geometry, measurements are limited by the necessary condition $\omega < \pm \theta$. Since Bragg angles for intense peaks (reliable peaks) are located in rather low θ-ranges, this limit is far below the necessary ranges of texture measurements. It is of course suited for low angle ranges, then for single crystals.

Now imagine a distribution of crystallite orientations which is not symmetric around **n** (Figure 10), for instance composed of two orientations with 0.1° FWHMs, one along **n** (with $\mathbf{c_1}$ axes), the other ($\mathbf{c_2}$ axes) at an angle χ from **n** and φ from the intersection of the sample surface and the scattering plane. Measured as positioned in Figure 10, a rocking curve on {00ℓ} planes will exhibit only one orientation component, C_1, the only one having {00ℓ} planes perpendicular to the scattering plane (Figure 6). The C_2 component will be revealed on a {00ℓ} rocking curve if the sample is rotated by φ around **n** before measurement (Figure 11).

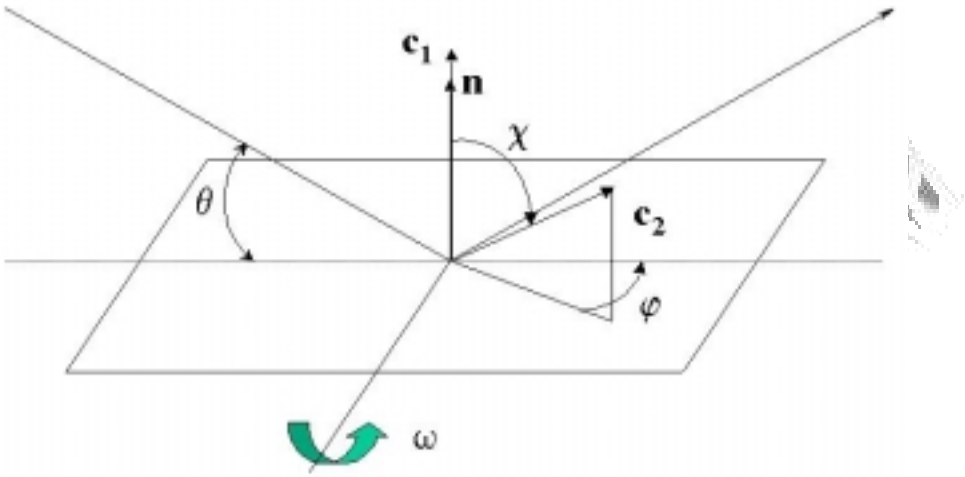

Figure 10: Two orientation components, represented by their **c** axes

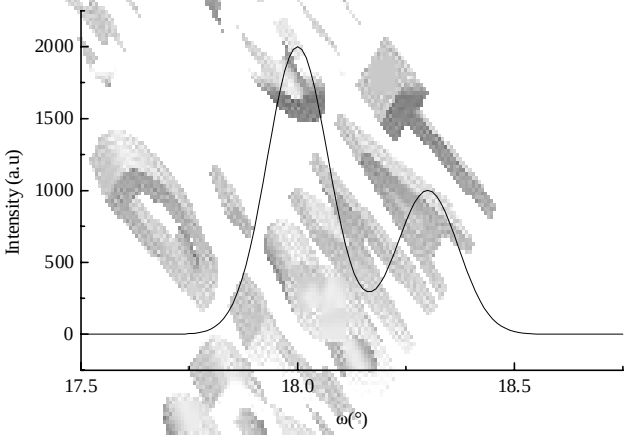

Figure 11: Two orientation components, Gaussians with 10° FWHMs, as described in Figure 10 after rotation of the sample by φ

We conclude in this paragraph that ω-scans can reveal the texture of a sample, with the absorption limitations discussed above, if several of these scans are measured in different φ orientations of the sample. This is exactly the goal of texture analysis !

5. Representations of textures: pole figures

5.1. Pole Sphere

Figure 12 represents a single crystallite orientation with the **c** axis at χ from **n**, and at φ from the macroscopic edges of the sample. The sphere on which all orientations can be distributed is also shown. This sphere of unit radius is called the Pole Sphere, with a $4\pi^2$ surface. The orientations can then be distributed over a solid angle of $4\pi^2$ sr at maximum. The intersection of the crystallographic direction [hkℓ] with the surface of the Pole Sphere is called a "pole", for instance the south or north poles !

In these representations, we are interested in the {hkℓ} planes distribution. We choose to locate the orientation of one (hkℓ) plane by its normal [hkℓ]*. Correlatively, all {hkℓ} planes will be located by their respective <hkℓ>* directions.

Except for single crystals, a material will contain numerous crystallites. A Pole Sphere of a polycrystal will be the representation of all the poles of all the crystallites of the sample. For cubic crystal structures, for which [hkℓ] $\perp$ {hkℓ}, the interpretation of the Pole Sphere is then straightforward, but for any other crystal system this relationship is not generally valid, and we may need the help of the reciprocal lattice construction.

As an evidence, plotting all the poles of all the {hkℓ} planes of all the crystallites of a sample would rapidly tend to a perfect homogeneous coverage of the Pole Sphere. Interesting information will be visible if we represent the poles for only one family of {hkℓ} planes. We will call this a {hkℓ} Pole Sphere. Also it may happen that experimentally several {hkℓ} plane families could not be separated, and we will have then a {hkℓ/h'k'ℓ'} Multipole Sphere.

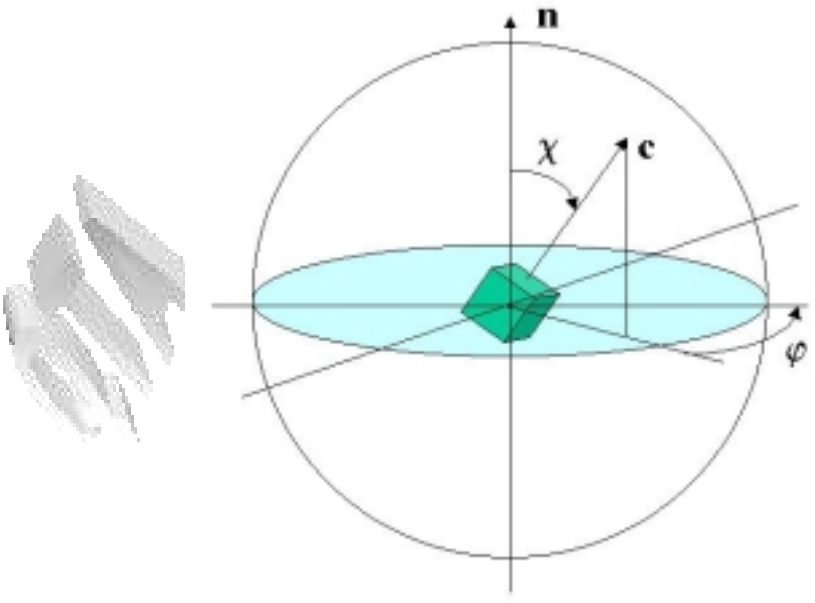

Figure 12: Representation of a crystallite orientation on the Pole Sphere

One entity which will be used is the unit surface element of the Pole Sphere, dS, the surface drawn for a (dχ, dφ) elementary variation. For a sphere of radius R, this elementary surface would be:

$$dS = R^2 \sin\chi \, d\chi \, d\varphi$$

which is in our case, with R = 1:

$$dS = \sin\chi \, d\chi \, d\varphi \qquad (3)$$

It is not very easy to represent a tri-dimensional object like a Pole Sphere and, although some programs can do it, to interpret them this way. Interpreting the Pole Sphere using two-dimensional projections is by far easier. We will call these projections {hkℓ} pole figures.

5.2. Stereographic projection

Figure 13a shows the stereographic projection of the pole sphere in the case of the single pole of Figure 12. A pole, P, representing the intersection of [hkℓ]* with the Pole Sphere, is projected on the equatorial plane in p, intersection of SP with the equatorial plane. In this projection, the φ angle is conserved. All points located at the same φ are describing a meridian (great circle) and all points at the same χ are at the same latitude (on a small circle). Hence a pole P(χ,φ) of the Pole Sphere is represented by the pole p(r',φ) in the {hkℓ} pole figure, where r' is the distance Op. Since r = R sinχ, we can plot a pole figure with any radius R using:

$$r' = R \tan(\chi/2)$$

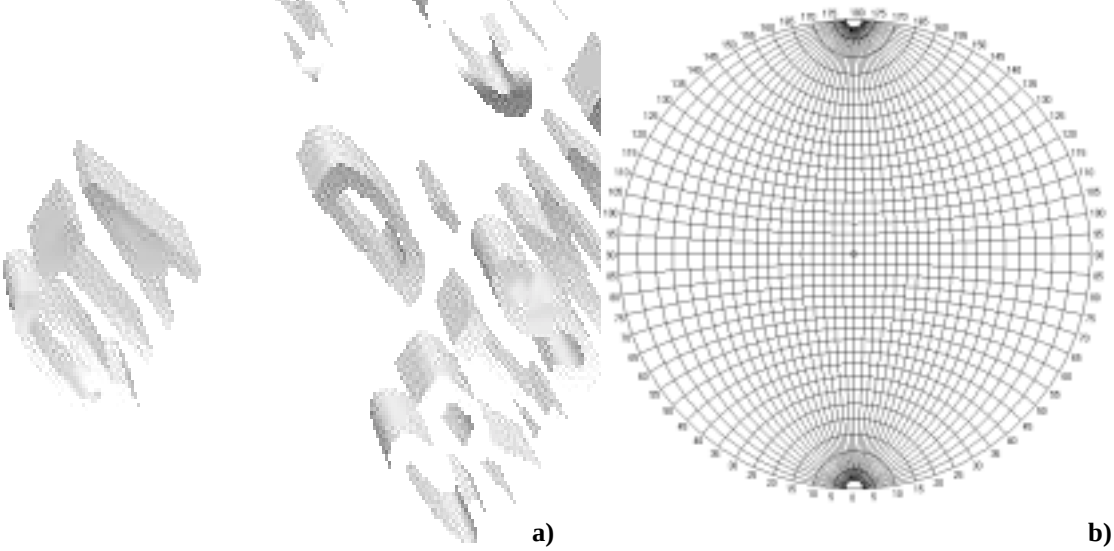

a) **b)**

Figure 13: Stereographic projection of Figure 12 (**a**) and Wulff net to manually read angles in the projection (**b**)

In such a projection, since tanχ is increasing with χ, two points located at the same angular distance Δχ on the sphere will be farther from one another near the periphery of the

projection than near its centre (Figure 15a). Then, randomly distributed points on the sphere will appear more concentrated in the centre of the projection. Also, the surface element (surface between four adjacent points) is larger for larger χ's.

Wulff nets (Figure 13b) may be used to manually determine angles between directions or planes on such projections.

5.3. Equal area projection: Lambert projection

The pole $P(\chi,\varphi)$ is projected on the plane tangent to the Pole Sphere containing the north pole (Figure 14), which is also conserving the φ angle. The rotation is around an axis perpendicular to the φ meridian passing by O, centre of the projection. The relation Op = OP is then valid for all points of the projection. For instance, a pole of the equator ($\chi = 90°$) will be at $R\sqrt{2}$ from O in the projection.

The projection $p(r',\varphi)$ can be obtained whatever R, after some geometry by:

$$r' = 2R \sin(\chi/2)$$

For a given increase in χ, the distance between two points of the projection will decrease slowly, particularly in the high χ-range. This decrease will partially compensate the increase in surface element due to φ. Then this surface element will be similar near the periphery and near the centre of the projection (Figure 15b), which is why this projection type is called "equal-area".

Schmidt nets may be used to manually determine angles between directions or planes on such projections.

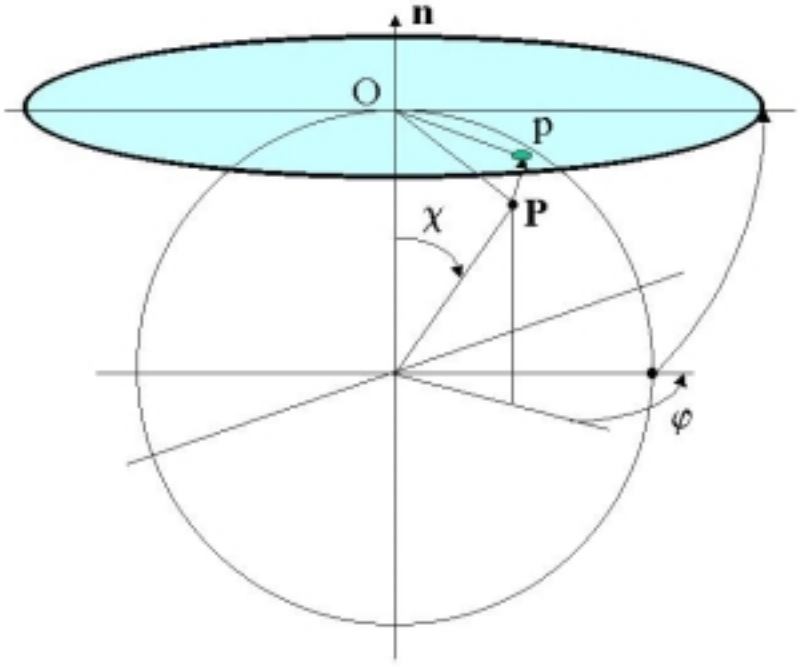

Figure 14: Lambert projection of Figure 12

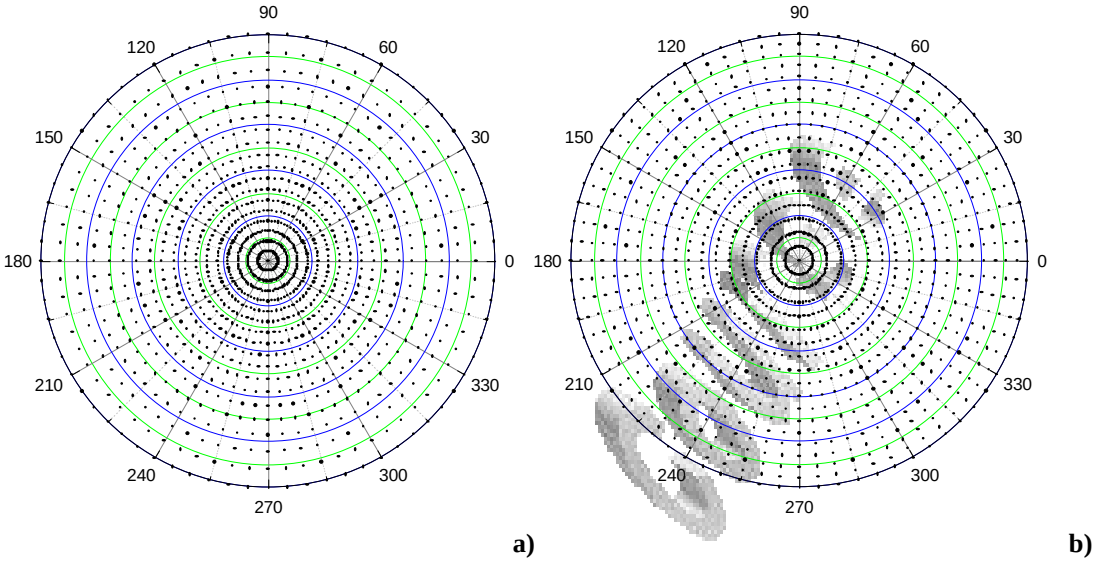

Figure 15: Stereographic (**a**) and Equal-area (**b**) projections of 1368 points located at every 5° in χ and φ on the Pole Sphere

5.4. Pole Figures

To each of the points of one {hkℓ} pole figure we will associate a diffracted intensity, $I_{hkl}(\chi,\varphi)$. Depending on the geometry of the experimental set-up, the angles χ and φ as measured on the diffractometer may need to be transformed in order to get the real pole figures. In all the following, we will reserve the angles χ and φ to the ones measured in the diffractometer (Spectrometer) space $\mathcal{S}$. After corrections, the angles retrieved in the pole figures space, $\mathcal{Y}$, will be ϑ_y and φ_y, or simply **y**. Similarly, since pole figures will represent <hkℓ>* direction distributions, we will simplify the notation into **h** = <hkℓ>*. Hence, on a Direct Pole Figure will be represented diffracted intensities $I_{\mathbf{h}}(\mathbf{y})$.

Since diffraction is depending on the density of the material (porosity, density of the phase in a polyphased material …), crystalline ratio (polymers …), thickness (thin films, multilayers …), diffraction yields (different planes diffract different intensities), particle sizes, stress/strain states …, it would become rapidly impossible to compare the orientation distributions between samples from direct pole figures. We then have to normalise these intensities into pole densities, or distribution densities, $P_{\mathbf{h}}(\mathbf{y})$. The resulting pole figures will be called Normalised Pole Figures.

While direct pole figures are showing diffracted intensities, in number of diffracted counts, the unity of normalised poles is the multiple of a random distribution, or m.r.d.. Using this unity, a sample without any preferred orientation will exhibit normalised pole figures with 1 m.r.d. for all **h** and **y**'s, i.e. $P_{\mathbf{h}}(\mathbf{y})$=1m.r.d.. A textured sample will show minima and maxima of densities, the minimum density being 0, the maximum infinity.

The unity abbreviation "mrd" is often used. Since it can be mistaken as "milli-radians", we choose to systematically use "m.r.d.".

6. Localisation of crystallographic directions from pole figures

6.1. Normal diffraction and pole figures

Pole figures are representations of the distributions of crystalline directions, as measured by diffraction in our case. In normal conditions for diffraction, i.e. far enough from the atomic absorption edges, (hkℓ) and ($\bar{h}\,\bar{k}\,\bar{\ell}$) planes are diffracting the same intensities (Friedel's law), at the same Bragg angle. It is then not useful to measure or represent the whole Pole Sphere, and only half of it, the upper hemisphere will be considered.

Of interest is the location of specific **h**'s in the sample that we are measuring. We need to associate to the sample a reference frame, which will be used in the pole figures. This sample reference frame, K_A, is made of three unit-vectors ($\mathbf{x_A}$, $\mathbf{y_A}$, $\mathbf{z_A}$) of the respective axes, X_A, Y_A, Z_A, such that $\mathbf{x_A} \wedge \mathbf{y_A} = \mathbf{z_A}$ (Figure 16). In order to simplify, we generally try to align these axes with macroscopic features of the sample. For instance, Z_A is positioned parallel to **n**, and the two other axes with the edges of the sample. The scattering plane is then perpendicular to (X_A, Y_A) in classical diffractometers. In K_A, a vector will be represented by its coordinates in terms of the unit-vectors ($\mathbf{x_A}$, $\mathbf{y_A}$, $\mathbf{z_A}$). For instance, the Z_A axis is co-linear to the vector **[001]** of the sample frame K_A. Note that the **[XYZ]** coordinates are bold characters, they have no correlation with the Miller indices which indicate crystal-related quantities.

Inside the sample are crystallites, having their own reference frame, K_B, with their own unit-vectors ($\mathbf{x_B}$, $\mathbf{y_B}$, $\mathbf{z_B}$) and axes, X_B, Y_B, Z_B (Figure 17). Similarly, we fix the normal to the diffracting plane of the crystallite, [hkℓ]*, parallel to Z_B. For crystal structures with right angles of the unit-cell (cubic, tetragonal and orthorhombic), X_B, Y_B, Z_B can be chosen parallel to **a**, **b**, **c** respectively, both frames having equal unit-vectors. However for other crystal systems, this is no longer the case, and the crystal structure will be needed to know the correspondence between K_B and **a**, **b**, **c**.

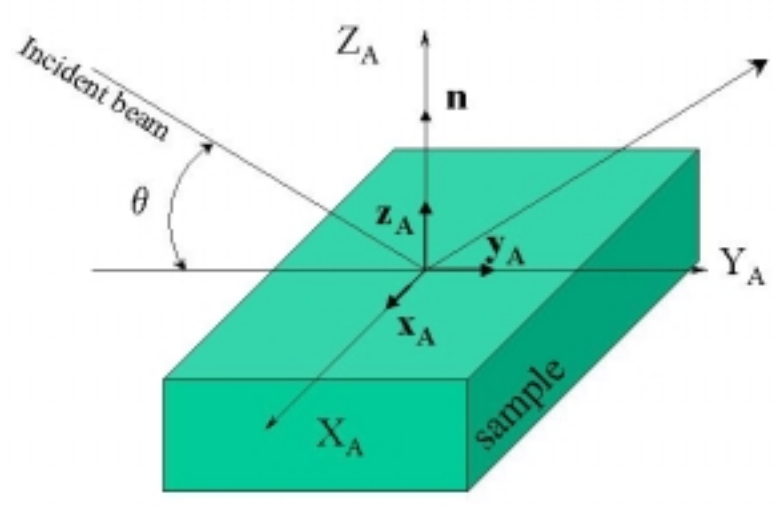

Figure 16: The sample reference frame $K_A = (\mathbf{x_A}, \mathbf{y_A}, \mathbf{z_A})$

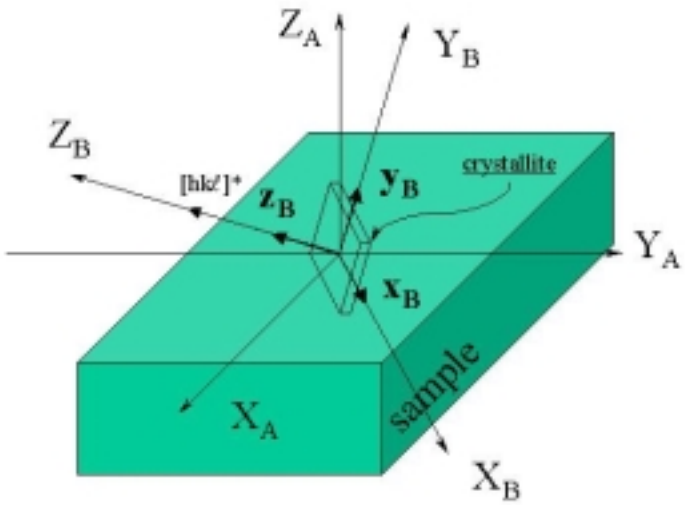

Figure 17: Crystal and sample reference frames $K_B = (\mathbf{x_B}, \mathbf{y_B}, \mathbf{z_B})$ and K_A respectively. Only one crystallite is shown

6.2. Grains, Crystallites and Crystallographic planes

Again, there is no relationship, *a priori*, between major axes of the crystallite and the K_B frame. In order to clarify the three notions crystallite/grain/diffracting planes, we represent in Figure 18 a two-dimensional cross-section of an hypothetical sample. The sample is made of grains, largest recognisable features in the cross section (green lines), which can vary in sizes and shapes, depending on the process of elaboration ... Inside each grain several crystallites (black or red lines) may appear, with various orientations, sizes and shapes, also depending on many factors. Crystallites inside a grain may be separated by coincidence site lattices, dislocation walls, twins, stacking faults, ... and it may happen that grains are constituted by only one crystallite. In this case, if only one grain constitutes the sample, we will call this peculiar sample a "single-crystal". Inside a crystallite, given (hkℓ) planes are strictly parallel. For three crystallites of Figure 18 we show crystallographic planes with different $d_{hk\ell}$ and different orientations.

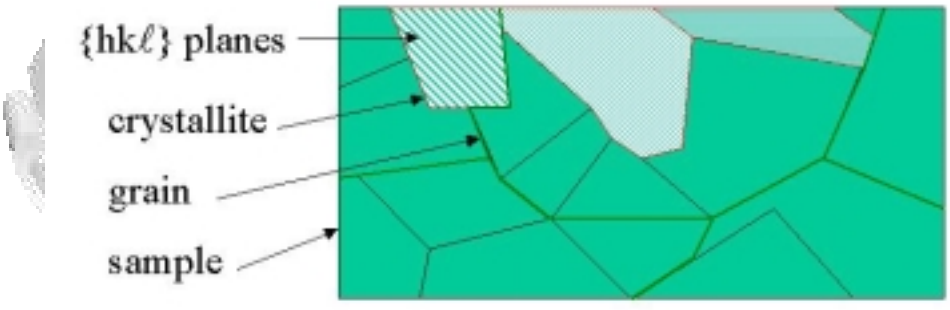

Figure 18: Definitions of grains (green), crystallites (black and red) and crystallographic planes (dashes)

The kind of relationship existing between grains, crystallites, crystallographic planes may be checked by local measurements with the help of electron microscopy, or by comparison between microscopy patterns and the QTA results.

6.3. Single texture component

In order to represent the textures, we will then use K_B and K_A in the pole figures. The pole figures will be represented in such a way that Z_A is their normal axis, X_A the horizontal axis and Y_A the vertical axis (Figure 19).

For one crystallite (Figure 19a), a direction **y** associated to the normal [hkℓ]* to the diffracting plane (hkℓ), is then localised by the polar angle ϑ_y and the Azimuthal angle φ_y. This latter takes its origin along X_A, and is taken positive for a left-handed rotation when looking down Z_A. It then respects the mathematical definition of K_A for a direct reference frame.

However, in a polycrystal, a large number of crystallites are diffracting, and the pole figure shows regions with large diffracted intensities (or densities, if we deal with normalised pole figures), indicating the tendencies of the crystallites to align around a given direction of the sample. The pole drawn by such an ensemble of crystallites (Figure 19b) is called a texture component. For one component, the pole enlarges around the previous **y** direction, meaning that some of the crystallites are about to align with **y**, but not strictly. It is then useful to describe the component by the same ϑ_y and φ_y angles as **y**, but giving the shape of the distribution and a parameter which quantifies how much the pole spreads, for instance Gaussian with 10° FWHM. But we should never forget that describing a pole by an analytical function imposes that we know the distribution is respecting the imposed shape, which is not easily verifiable. For instance, in thin films, poles may appear very much elongated in one direction, but not in the other (Pernet et al. 1994) due to the substrate interaction with the film. Also, distributions may exhibit shapes which are other than Gaussian, Lorentzian for instance (Isaure et al. 2001).

The diffraction intensity (then density) will depend on how the dispersion is for a given pole. The larger the dispersion the lower the diffraction will be. The intensity and density values are represented by colour or contour levels. However, for now, we have not normalised the pole figures into quantitative densities, and it is not necessary to indicate these intensity scales.

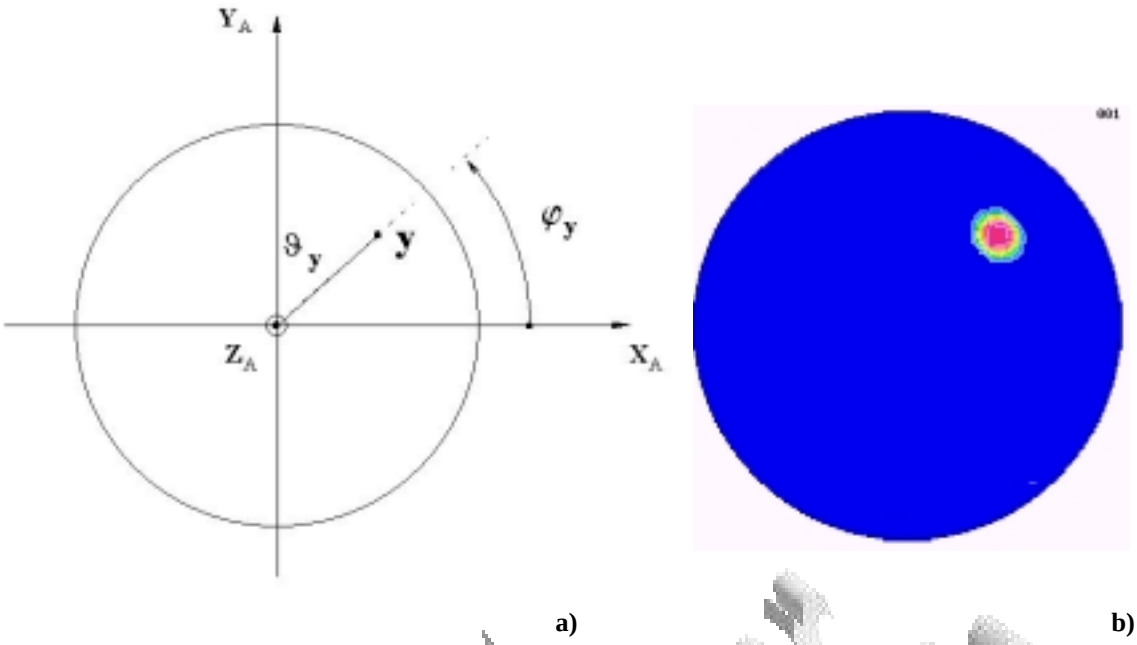

a) **b)**

Figure 19: a): $P_{\mathbf{h}}(\mathbf{y})$ Diffraction pole figure for one crystallite. The direction **y** is associated to the [hkℓ]* normal. **b)**: Pole figure of a texture component centred on the previous **y**, having a Gaussian shape of 10° FWHM, for **h** = <001>* of an orthorhombic crystal structure.

6.4. Multiple texture components

Several components of texture may be present, as was the case in Figure 10. We have taken this bi-component example and represented it in Figure 20 for $\mathbf{c_1}$ axes located around ($\vartheta_y = 0$; $\varphi_y = 0$) and $\mathbf{c_2}$ axes around ($\vartheta_y = 15°$; $\varphi_y = 300°$). On this figure we now clearly see that an ω-scan measured with the scattering plane containing Z_A and X_A (horizontal dashed line) will exhibit a rocking curve with a single peak as in Figure 6 (but with a FWHM of 10°, if corrected for absorption variations), which reveals to be very poor to describe the actual texture !

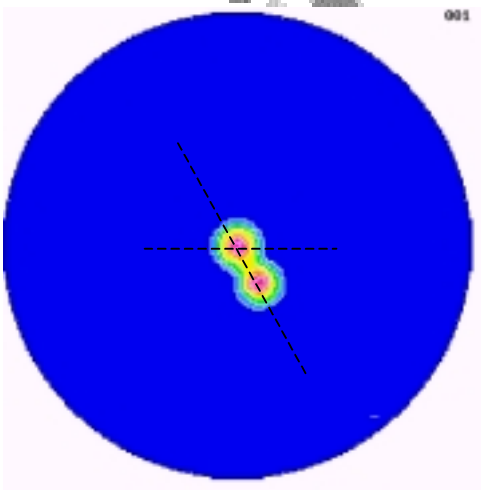

Figure 20: {001} pole figure for the two-components texture of Figure 10. Each component has 10° FWHM, $\mathbf{c_1}$ being centred ($\vartheta_y = 0$; $\varphi_y = 0$) and $\mathbf{c_2}$ being located at ($\vartheta_y = 15°$; $\varphi_y = 300°$)

Now rotating the scattering plane by 300° in φ, then measuring the ω-scan (oblique dashed line), will provide the Figure 10, which correctly represents the bi-component texture (knowing the shape can be represented by two Gaussians).

6.5. Pole figures and (hkℓ) multiplicity

Using diffraction, all the (hkℓ) diffracting at the same Bragg angle will be retrieved on the same $P_{\mathbf{h}}(\mathbf{y})$ pole figure. For instance (123) and (321) in a cubic crystal system. Then the pole figure has to reveal the line multiplicity. Taking the C_1 component of Figure 20 but with a cubic crystal structure will give the pole figure of Figure 21, with one full pole (001) and four halves (corresponding to (100) and (010)) at 90° in ϑ_y from (001). The multiplicity of this pole figure is three at total, while the crystallographic multiplicity of the (100) reflection of a cubic crystal system is six. Since we only concern the upper hemisphere in normal diffraction pole figures, this is coherent.

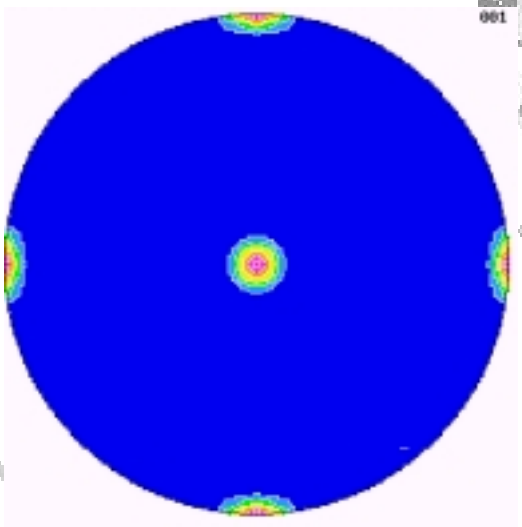

Figure 20: {001} pole figure for the component C_1 of Figure 20, for a cubic crystal structure

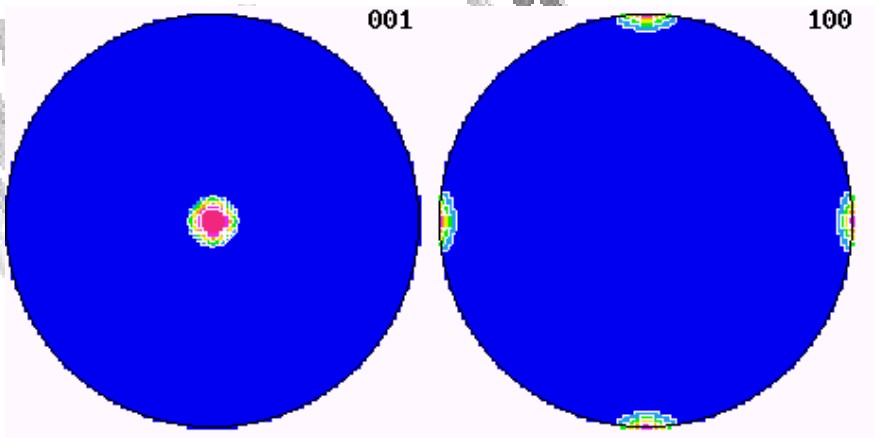

Figure 21: Pole figures for the C_1 component for a tetragonal crystal system. **a)**: {001} **b)**: {100}

Then, for a given crystal system, two pole figures of different multiplicity will exhibit a different number of poles. For instance (Figure 21), a sample crystallising in a tetragonal crystal system which possess the C_1 component will exhibit a {001} pole figure with only one pole while the {100} will exhibit four halves.

6.6. A real example

As we have seen in the just previous paragraphs, a pole figure can then be a complex object to interpret. It is a combination of a multiplicity, of components, with more or less regular dispersions. Figure 22 shows pole figures which are combining many of these effects. They have been measured on a real sample, an aragonite layer from the sea shell (a cowry) *Cypraea testudinaria*. These pole figures are combining twinning, dispersion and two components, of the orthorhombic crystal system (Chateigner et al. 1996).

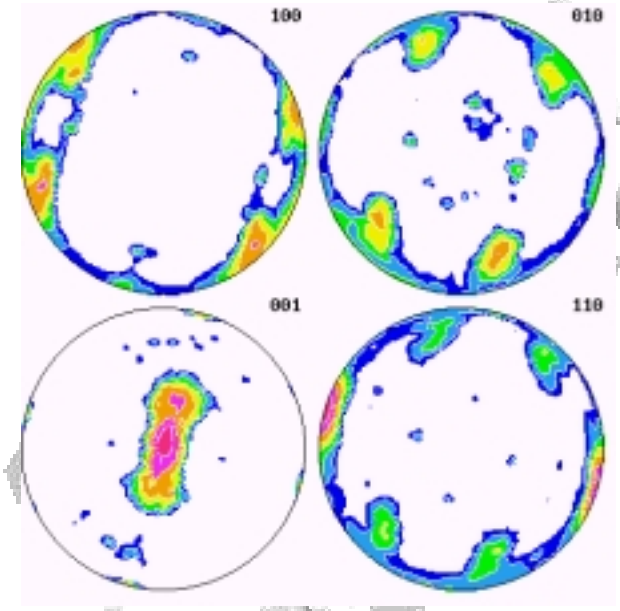

Figure 22: {100}, {010}, {001} and {110} pole figures of an aragonite (orthorhombic crystal system) layer from the sea shell *Cypraea testudinaria*

As we see, it is not easily interpretable at once, and we will need tools to help us. As a first approach, we will classify the different texture types that one can encounter.

7. Texture types

7.1. Random texture

A random texture (or random sample) is simply a name given to the texture exhibited by a sample that has no preferred orientation. Its crystallites are randomly distributed in orientation. Then, statistically, there is the same number of grains diffracting at any **y**, and the collected diffracted intensity for any **y** point in the pole figure is the same. Consequently, any given crystalline {hkℓ} planes are also randomly distributed, and all the pole figures are

homogeneous, whatever **h**, and whatever the crystal system. In such a texture, each crystallite has three degree of freedom (rotations around three orthogonal axes) to position K_B relative to K_A. Figure 23 shows the {100}, {001} and {110} pole figures of a random sample.

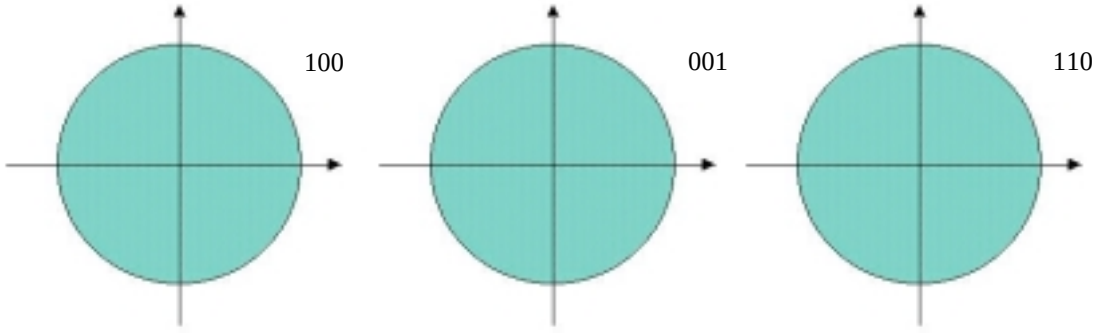

Figure 23: {100}, {001} and {110} pole figures of a random sample. Three degrees of freedom to orient each crystallite

7.2. Planar textures

This kind of texture is exhibited by samples in which crystallites have two degrees of freedom to orient. One specific <hkℓ>* direction family was allowed to rotate around one sample axis. Then the <hkℓ>* directions are located in a plane, perpendicular to the rotation axis, any other crystal direction around the given <hkℓ>* being at random. This is called a planar texture. Imagine the rotation axis is X_A and the direction family <100>* of an orthorhombic crystal system (Figure 24). The <100>* directions are then distributed in the (Y_A, Z_A) plane. But since other directions are at random around <100>*, their pole figures remain homogeneous.

Of course, it is a peculiar case that the rotation axis is along a major axis of the sample, and that <100>* (**a** axes) are the concerned directions. It could have been an inclined axis of rotation, and reflections with a larger multiplicity, giving rise to more complex pole figures. Planar textures with the rotation axis around Z_A are called cyclic-planar texture (Figure 25).

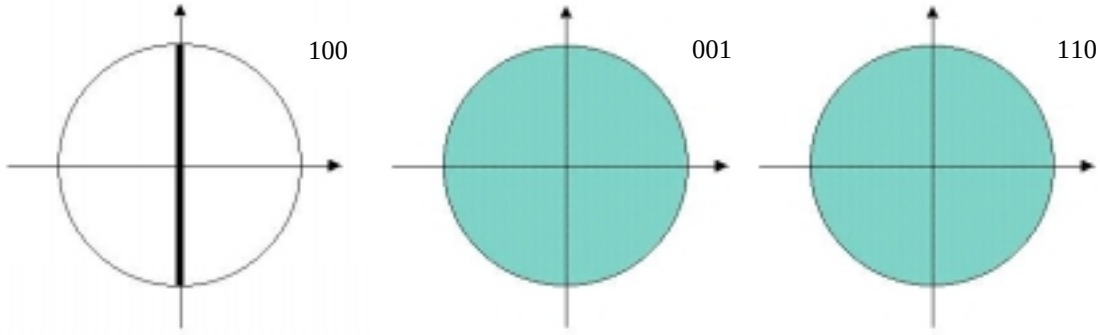

Figure 24: {100}, {001} and {110} pole figures of a planar texture of the orthorhombic crystal system. Rotation axis of the planar texture is with <100>* directions perpendicular to X_A

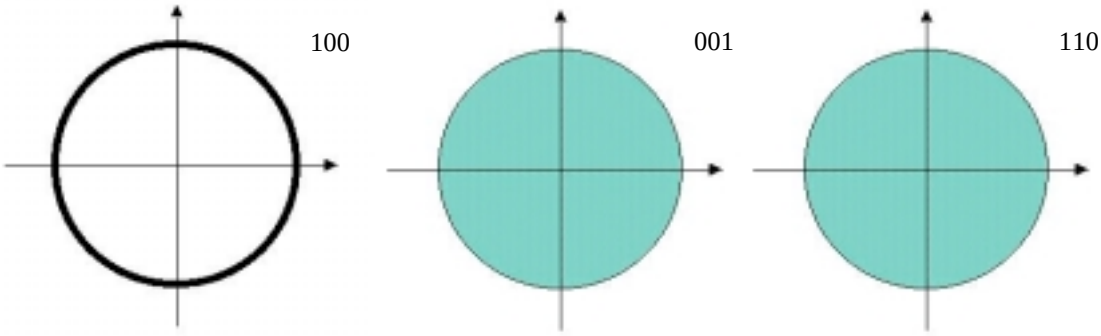

Figure 25: {100}, {001} and {110} pole figures of a cyclic-planar texture of the orthorhombic crystal system. Rotation axis of the cyclic-planar texture is with <100>* directions perpendicular to Z_A

7.3. Fibre Textures

If the crystallites loose another degree of freedom in their orientation, they are forced to align one of their <hkℓ>* with one direction of the sample, all other directions being at random around <hkℓ>*. Such a texture is called fibre texture.

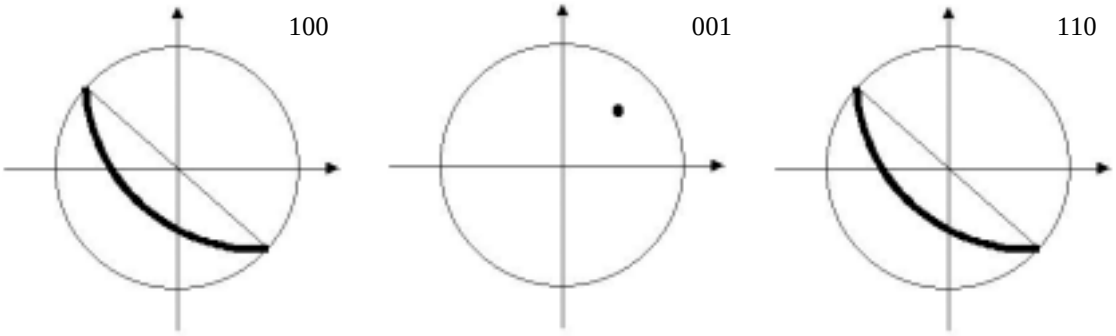

Figure 26: {100}, {001} and {110} pole figures of a fibre texture of the orthorhombic crystal system. Fibre axis is with <001>* directions at (ϑy = 45°; φy = 45°)

For instance, imagine all the <001>* from an orthorhombic crystal system are located along (ϑ_y = 45°; φ_y = 45°) (Figure 26). Then <100>* and <110>* directions will be located at random on a plane perpendicular to this **y**.

Similarly as previously, if the <001>* directions are aligned with Z_A, then the texture is called cyclic-fibre texture (Figure 27). Such a texture has <100>* and <110>* poles located on the periphery of the equator.

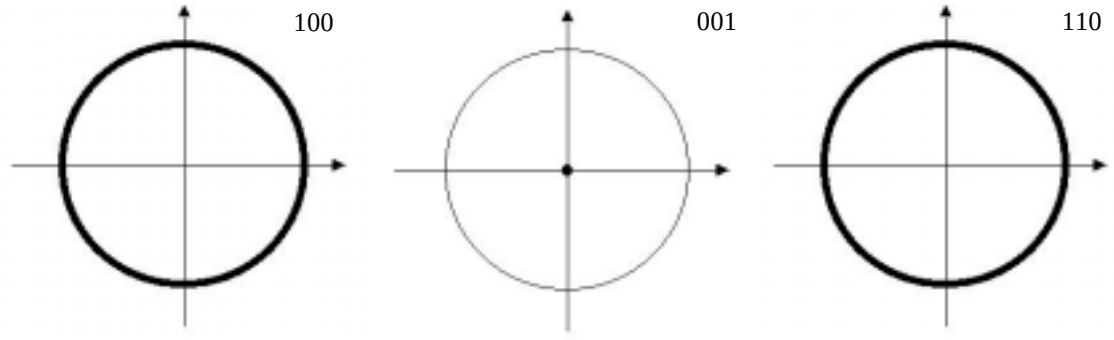

Figure 27: {100}, {001} and {110} pole figures of a cyclic-fibre texture of the orthorhombic crystal system. Fibre axis is with <001>* directions along Z_A

7.4. Three-dimensional texture

Samples composed of crystallites which had no choice to orient themselves in K_A (0 degree of freedom) will exhibit punctual poles for all their pole figures. The pole figures will be similar to the ones of a single crystal. We call this texture 3D texture. If, for instance, the <001>* are aligned with Z_A, and the <100>* with X_A, the pole figures will look like in Figure 28. The φ_y angle to which are localised the <110>* poles depends, for an orthorhombic crystal system, on the c/a ratio of the material phase.

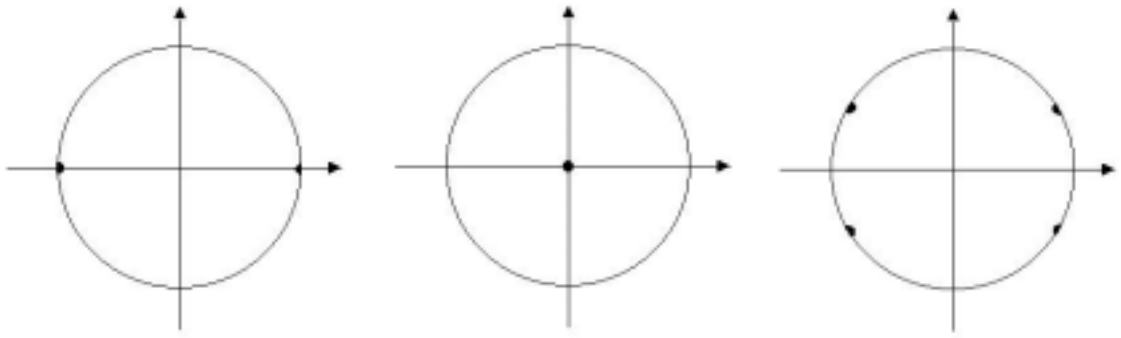

Figure 28: {100}, {001} and {110} pole figures of a 3D texture of the orthorhombic crystal system, with <001>* directions along Z_A and <100>* directions along X_A

One should avoid at this point to confuse between a real single crystal and a polycrystal having all its crystallites perfectly aligned one with each other, as in a single crystal (Figure 29). The diffracted intensity is proportional to the square of the number of planes that build up the crystallite in the $\mathbf{\Delta k}$ direction. In the former case this number is large (it is the single crystal size in this direction), while in the latter case each crystallite in restricted in size and the number of planes is small. The diffracted intensity is then much larger for a single crystal, and direct pole figures will show very large intensity in this case, although crystallites may be perfectly aligned in the polycrystal. However, in the normalised pole figures, this difference will disappear since such figures only take into account the orientation distributions.

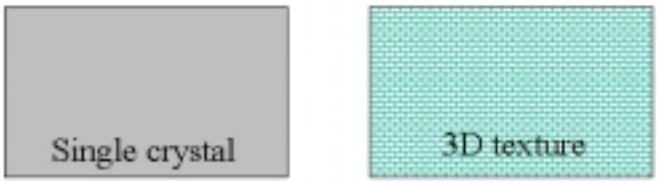

Figure 29: Difference between a perfect single crystal and a polycrystal having perfect 3D crystallite orientations. Normalised pole figures would be identical

8. Pole Figures and Orientation spaces

8.1. Pole figures and orientation of planes

Figure 8 already showed us the ambiguity of the diffraction to reveal the orientation of planes: there is no difference in the diffracted intensity between two orientation components only differing by their rotation around **Δk** (or **n** in Figure 8). Since in diffraction **Δk** is aligned with the vector **h**, planes oriented in such a way that **h** is parallel to a certain direction **y** will all diffract, whatever their orientation around **y**. Differently said, diffraction only probes a direction, not an orientation, and we need at least to determine the location of two direction of a plane to know its orientation.

An example was given already, but implicitly, in Figure 27 for the cyclic-fibre texture. In this figure, all the pole figures are different representations, as viewed from a different **h**, of the same sample. Planes that contribute to the {001} pole are crystallographically linked to the ones distributed on the periphery of the {100} and {110} pole figures. A crystallite which has {001} planes (orthorhombic crystal symmetry) diffracting at the centre of the {001} pole figure will have {100} planes diffracting on the periphery of the {100} pole figure since these planes are at 90° from each other in the crystal.

Imagine now that only the {001} pole figure is accessible experimentally, with the same pattern as in Figure 27. The information that gives such a figure is: c-axes of the crystallites are all aligned with Z_A. But nothing is given on the a-axes for instance, except that they are at 90° of the c-axes and will give a signal on the periphery of the {100} pole figure. In particular, nothing will dissociate in this theoretical case between a fibre-like texture (Figure 27) or a 3D texture (Figure 28) having the same c-axes orientation.

8.2. Mathematical expression of diffraction pole figures

Diffraction measurements give in the $\mathscr{Y}$ space the pole figures, $P_{\mathbf{h}}(\mathbf{y})$ (Figure 19a) after proper geometrical transformations from the $\mathscr{S}$ space. They represent the volumic volumic density of crystallites oriented in **dy**, i.e. between (ϑ_y, φ_y) and $(\vartheta_y + d\vartheta_y, \varphi_y + \varphi_y)$. This can be expressed by:

$$\frac{dV(\mathbf{y})}{V} = \frac{1}{4\pi} P_{\mathbf{h}}(\mathbf{y})\, \mathbf{dy} \qquad (4)$$

where V is the irradiated volume (in diffraction experiments) of the sample and dV(**y**) the volume of crystallites which orientation is with **h** directions between **y** and **y**+**dy**.

Similarly to Equation 3 and for consistency we have:

$$\mathbf{dy} = \sin\vartheta_y \, d\vartheta_y \, d\varphi_y \tag{5}$$

The factor $1/4\pi$ standing for normalising the pole figure into distribution densities, which necessitates a normalisation condition for each pole figure:

$$\int_{\varphi_y=0}^{2\pi} \int_{\vartheta_y=0}^{\pi/2} P_{\mathbf{h}}(\vartheta_y, \varphi_y) \sin\vartheta_y \, d\vartheta_y \, d\varphi_y = 4\pi \tag{6}$$

8.3. The Orientation space

As just illustrated, the orientation of planes is defined by locating at least two directions in the space. We then need another concept, the Orientation Distribution Function (or ODF), f(g).

This function, analytical or not, represents the statistical distribution of the orientations of the crystallites in a polycrystalline aggregate. It is defined similarly as the pole figures by:

$$\frac{dV(g)}{V} = \frac{1}{8\pi^2} f(g) \, dg \tag{7}$$

where $dg = \sin(\beta) d\beta d\alpha d\gamma$ is the orientation element (defined in a 3-dimensional space), defined by three Euler angles, $g=\alpha,\beta,\gamma$ (Figure 30) in the orientation space (or -space).

These three Euler angles bring the crystal coordinate system K_B colinear with the sample coordinate system K_A. The -space can be constructed from the space groups, taking into account their rotation parts (since orientations are rotations) and the inversion centre (since we are using diffraction). The two first angles α and β determine generally the orientation of the $<001>^*$ crystallite directions in K_A, they are called azimuth and colatitude (or pole distance) respectively. The third angle, γ, defines the location of another crystallographic direction, chosen as <010>* (or b in the (a,b) plane of an orthogonal crystal system). V is the irradiated volume of the sample, dV(g) the volume of crystallites which orientation is between g and g+dg.

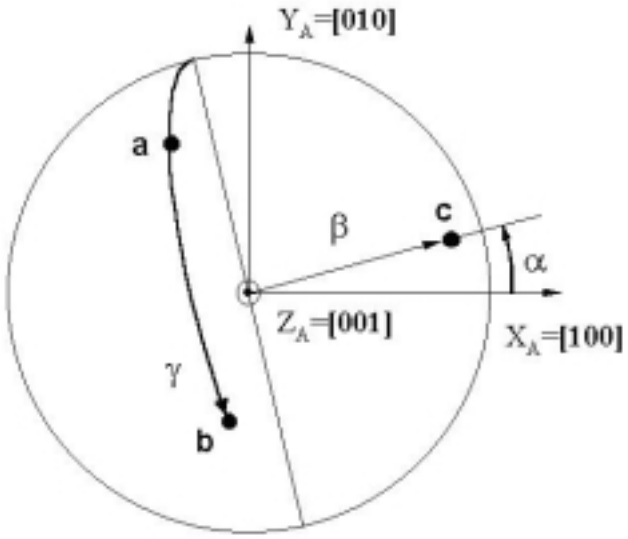

Figure 30: Definition of the three Euler angles that define the position of the crystallite coordinate system K_B of an orthogonal crystal cell in the sample coordinate system K_A.

The function f(g) then represents the volumic density of crystallites oriented in dg. It is also measured in m.r.d. and normalised to the value $f_r(g)=1$ for a random sample. The normalisation condition of f(g) over the whole orientation space is expressed by:

$$\int_{\alpha=0}^{2\pi}\int_{\beta=0}^{\pi/2}\int_{\gamma=0}^{2\pi} f(g)\,dg = 8\pi^2 \qquad (8)$$

The function f(g) can take values from 0 (absence of crystallites oriented in dg around g) to infinity (for some of the $\mathcal{H}$-space values of single crystals).

8.4. Euler angles conventions

There is an infinite number of possibilities for the choice of the Euler angles. The two most used choices are the Roe-Matthies (Roe 1965, Matthies et al. 1987) and the Bunge (Bunge et Esling 1982) conventions. A "symmetric Euler angles" set has been described by Kocks 1988, and another convention by Canova et Kocks 1984.

In the Roe-Matthies and Bunge conventions, we use the so-called "rotation method". In these methods, K_A is rotated through three angles in order to bring it colinear to K_B, or inversely, respectively for the two conventions. For instance, in the Roe-Matthies frame, K_A is brought coincident to K_B by the operation $g : [K_A \mapsto K_B]$, using the three following rotations:

- Rotation of K_A about the axis Z_A through the angle α:
  $[K_A \mapsto K'_A]$; associated rotation $g_1 = \{\alpha,0,0\}$
- Rotation of K'_A about the axis Y_A through the angle β:
  $[K'_A \mapsto K''_A]$; associated rotation $g_2 = \{0,\beta,0\}$
- Rotation of K''_A about the axis Z''_A through the angle γ:
  $[K''_A \mapsto K'''_A//K_B]$; associated rotation $g_3 = \{0,0,\gamma\}$

we obtain finally:

$$g = g_1\, g_2\, g_3 = \{\alpha,0,0\}\ \{0,\beta,0\}\ \{0,0,\gamma\} = \{\alpha,\beta,\gamma\}$$

The other set of rotation defined by Bunge uses three other angles, $g = \{\varphi_1,\Phi,\varphi_2\}$ which simply differs in the second rotation step, which is operated about X'_A instead of Y'_A. Table 1 shows the angular correspondences for the four most used conventions.

Matthies	Roe	Bunge	Canova	Kocks
α	Ψ	$\varphi_1 = \alpha + \pi/2$	$\omega = \pi/2 - \alpha$	Ψ
β	Θ	Φ	Θ	Θ
γ	Φ	$\varphi_2 = \gamma + 3\pi/2$	$\phi = 3\pi/2 - \gamma$	$\Phi = \pi - \gamma$

Table 1: Correspondences between the most used Euler angle sets

8.4. Orientations and Pole figures

From the definition of the Roe-Matthies convention it can be seen that the angles α and β correspond simply to the angles ϑ_y and φ_y of the pole figures. From the pole figures, we then just have to imagine the third angle γ of the orientation, which is why we decided here to use exclusively this convention.

Lets take few examples in order to finish this part, for an orthorhombic crystal system. An orientation component centred on the $g = \{0,0,0\}$ will have K_A and K_B perfectly aligned on each other, which is the situation of Figure 28 with the same pole figures. Starting from this situation, a rotation {45°,0,0} will give the {001/100/010} multipole figure of Figure 31a. Then, a rotation {45°,45°,0} will be represented by the {001/100/010} multipole figure of Figure 31b, and a {45,45,55} rotation the one of Figure 31c.

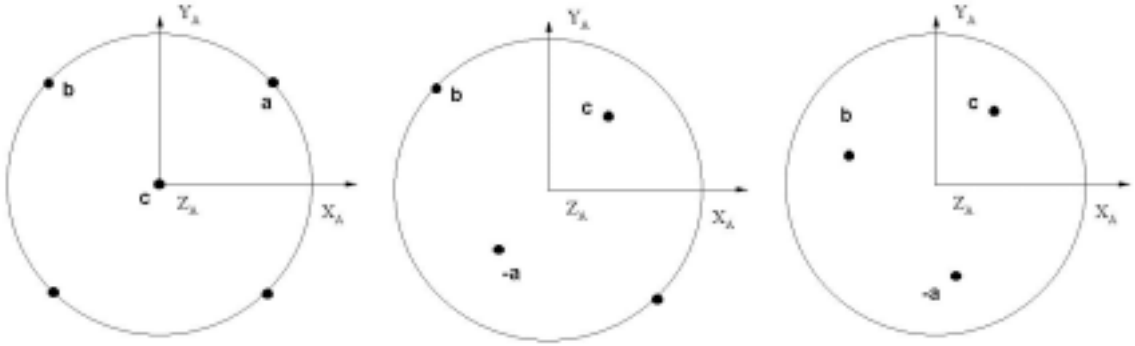

a) **b)** **c)**

Figure 31: {001/100/010} multipole figures for an orthorhombic crystal structure for the orientations **a)**: {45,0,0}; **b)**: {45,45,0}; **c)**: {45,55,45}. Roe-Matthies convention

References

Brentano J.C.M. 1946. Parafocusing properties of microcrystalline powder layers in x-ray diffraction applied to the design of x-ray goniometers. *J. of Applied Physics* **17** 420-434.

Canova G.R., Kocks U.F. 1984. The development of deformation textures and resulting properties of fcc metals. In "7th International Conference on Textures of Materials", Brakman C.M., Jongenburger P., Mittemeijer E.J. eds. Netherlands, Society for Materials Science, p573-579.

Chateigner, Hedegaard C., Wenk H.-R. 1996. Texture analysis of a gastropod shell: Cypraea testudinaria. In "11th International Conference on Textures of Materials", *Ed. Z. Liang, L. Zuo & Y. Chu, Int. Academic Publishers* **Vol. 2** 1221-1226.

Field M., Merchant M.E. 1949. Reflection method of determining preferred orientation on the Geiger-counter spectrometer. *J. of Applied Physics* **20** 741-745.

Heizmann, J.-J., Laruelle, C. (1986). Simultaneous measurement of several x-ray pole figures. *Journal of Applied Crystallography* **19** 467-472.

Isaure M.-P., Laboudigue A., Manceau A., Sarret G., Tiffreau C., Trocellier P., Lamble G., Hazemann J.-L., Chateigner Daniel 2002. Quantitative Zn speciation in a contaminated dredgeg sediment by μ-PIXE, μ-EXAFS spectroscopy and principal component analysis. *Geochimica et Cosmochimica Acta* **66** 1549-1567.

Kocks U.F. 1988. A symmetric set of Euler angles and oblique orientation space sections. In "8th International Conference on Textures of Materials", Kallend J.S. et Gottstein G. eds. Warrendale, PA, USA: The Metallurgical Society, p31-36.

Lotgering F.K. 1959. Topotactical reactions with ferrimagnetic oxides having hexagonal crystal structures-I. *J. of Inorganic and Nuclear Chemistry* **9** 113-123.

Pernet M., Chateigner D., Germi P., Dubourdieu C., Thomas O., Sénateur J.-P., Chambonnet D., Belouet C. 1994. Texture influence on critical current density of YBCO films deposited on (100)-MgO substrates. *Physica C* **235-240** 627-628.

Roe R.-J. 1965. Description of crystallite orientation in polycrystalline materials III, general solution to pole figure inversion. *J. of Applied Physics* **36** 2024-2031.

Wcislak L., Bunge H.-J., Nauer-Gerhardt C.U. 1993. X-ray diffraction texture analysis with a position sensitive detector. *Zeitschrift für Metallkunde* **84(7)** 479-493.

Wenk H.-R. 1998. Pole figure measurements by diffraction techniques. In "Texture and Anisotropy", Kocks U.F., Tomé C.N., Wenk H.-R. (Eds), Cambridge University Press, pp 167-177.

Wright Stuart I. (1993). A review of automated orientation imaging microscopy (OIM). *J. of Computer-Assisted Microscopy* **5(3)** 207-221.

Wright Stuart I., Adams Brian L. (1992). Automatic analysis of electron backscatter diffraction patterns. *Metallurgical transactions A, Physical metallurgy and materials science* **23(3)** 759-767.

